JACS
JOURNAL OF THE AMERICAN CHEMICAL SOCIETY

Communication

pubs.acs.org/JACS

Quantitating the Lattice Strain Dependence of Monolayer Pt Shell Activity toward Oxygen Reduction

Xiaoming Wang,*[,†] Yuki Orikasa,[†] Yuki Takesue,[‡] Hideo Inoue,[§] Masashi Nakamura,[‡] Taketoshi Minato,[∥] Nagahiro Hoshi,[‡] and Yoshiharu Uchimoto[†]

[†]Graduate School of Human and Environmental Studies, Kyoto University, Sakyo-ku, Kyoto 606-8501, Japan

[‡]Graduate School of Engineering, Chiba University, Inage-ku, Chiba 263-8522, Japan

[§]Ishifuku Metal Industry Limited Company, Soka-shi, Saitama 340-0002, Japan

[∥]Office of Society-Academia Collaboration for Innovation, Kyoto University, Uji-shi, Kyoto 611-0011, Japan

Supporting Information

ABSTRACT: Lattice strain of Pt-based catalysts reflecting d-band status is the decisive factor of their catalytic activity toward oxygen reduction reaction (ORR). For the newly arisen monolayer Pt system, however, no general strategy to isolate the lattice strain has been achieved due to the short-range ordering structure of monolayer Pt shells on different facets of core nanoparticles. Herein, based on the extended X-ray absorption fine structure of monolayer Pt atoms on various single crystal facets, we propose an effective methodology for evaluating the lattice strain of monolayer Pt shells on core nanoparticles. The quantitative lattice strain establishes a direct correlation to monolayer Pt shell ORR activity.

The commercialization of proton exchange membrane fuel cells (PEMFCs) can help to mitigate global warming and reduce our dependence on fossil fuels. However, efficient cathodic electrocatalysts for oxygen reduction are largely unavailable,[1,2] and so fundamental progress in the design of these catalysts is highly needed. Recently, the rise of monolayer Pt system with more flexible design provides a promising approach to reduce Pt usage and enhance Pt catalysis toward oxygen reduction reaction (ORR).[3] Considering their practical application in fuel cells, more and more interests focus on the complete synthetic control of surface properties in monolayer Pt shells for the greater activity.[4−6] The status of d-band in monolayer Pt surfaces modified by ligand and strain effects regulates the adsorption properties of rate-limiting intermediates and eventually decides the catalytic properties.[7] Herein, ligand effect is caused by the atomic vicinity of two dissimilar surfaces that induces electronic charge transfer between them, and strain effect is generated by the atomic arrangement of the surface layer to form a compressed or expanded structure (surface strain). Generally, ligand and strain effects simultaneously impact the observed catalytic reactivity. Considering the dimensions across which ligand and strain effects are effective, only geometric strain can impact surface reactivity over more than a few atomic layers,[8] as demonstrated in Pt alloyed and dealloyed systems.[9,10] Thus, for monolayer Pt shells, how to quantitatively assess their lattice strain to establish a direct correlation to ORR activity is the kernel of the complete synthetic control for optimal catalytic performance.

Quantitative extended X-ray absorption fine structure (EXAFS) analysis derived from X-ray absorption spectroscopy (XAS) provides us a valuable tool to explore the lattice strain of various systems, such as Pt nanoparticles and Pt-based alloys.[11] Generally, EXAFS analysis taken in fitting the sample data involves building the structural model, calculating the referenced parameters, and fitting the experimental data (Figure S1). Among them, the structural model plays the decisive role in the fitting quality of EXAFS data. For Pt nanoparticles and Pt-based alloys with the long-range ordering structure, their uniform crystal structure can be employed as the structural model to obtain the referenced parameters, and then the following EXAFS fitting gets their real local structure. However, for monolayer Pt shells on core nanoparticles with the short-range ordering structure, since the real structure contains various structural units on different core facets, such as (111), (100), and (110), how to build the structural model encounters an impassable chasm. Thus, in previous publications about (in situ) XAS investigation of monolayer Pt shells, only qualitatively structural analysis has been done.[12,13] In this regard, although some groups have attempted to get the local structure of monolayer shells using different ways,[14−16] the prevalence of their methods is undermined by the intangible structural model of monolayer shell, the absent validation of the proposed structural model using the standard monolayer samples, or the complicated procedure.

In this work, based on EXAFS analysis of monolayer Pt atoms on various Pd single crystal facets, we propose a general methodology for evaluating the lattice strain of monolayer Pt shells on Pd core nanoparticles. And then, we investigate the lattice strain of monolayer Pt shells on a variety of Pd nanoparticles. Further, the lattice strain dependence of the resulting ORR activity has been studied.

As discussed above, in EXAFS fitting of monolayer Pt shells on core nanoparticles, it is difficult to build a general structural model which contains all structural information on different core facets. Thus, it is necessary to get some correlations among these monolayer structures on different core facets. First, it

Received: December 19, 2012
Published: April 5, 2013

   dx.doi.org/10.1021/ja312382h | J. Am. Chem. Soc. 2013, 135, 5938−5941

should be noted, it is acceptable that the practical EXAFS fitting is performed only for the nearest neighbors,[14−16] although the amplitudes in EXAFS spectrum ascribe to the backscattering contribution of different shell neighbors. The above approximate treatment is based on the fact that the backscattering contribution from the neighbors at longer distances causes an apparent amplitude reduction of the radial structure function for higher shells, as predicted by the EXAFS equation (Figure S2). In the case of EXAFS spectrum of monolayer Pt shells, the above phenomenon is particularly evident due to the feeble signal derived from the ultralow Pt amount and the two-dimensional structure (Figure S2). In Figure S3 and Table S1, we further investigate the practical influence of the backscattering contribution from the second- and third-shell neighbors at longer distances and demonstrate that EXAFS fitting only for the nearest neighbors will generate the neglectable discrepancy in the obtained structural parameters. Thus, for monolayer Pt shells, their EXAFS fitting will be carried out only for the nearest neighbors. And then, comparing the nearest neighbors (green dashed frame in Figure 1a) on different core facets, we can easily find that they remain essentially the same despite all apparent changes, where Pt−Pt and Pt−Pd neighbors are same and the corresponding coordination number and bond distance are different. For the nearest neighbors, in evidence, monolayer Pt atoms on (100) and (110) facets can be seen as the defective structure of monolayer Pt atoms on (111) facet (Figure 1a).

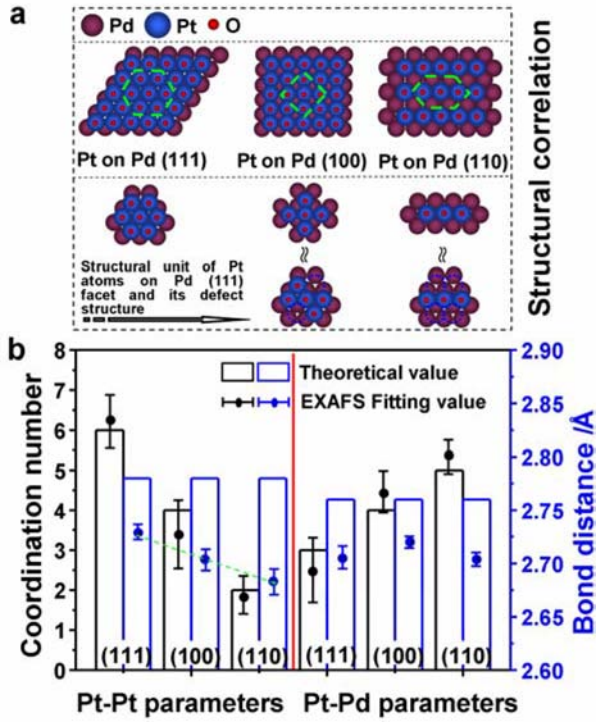

Figure 1. Proposition of a general structural model for EXAFS fitting of monolayer Pt shells on core nanoparticles. (a) Structural resemblance of the nearest neighbors in monolayer Pt shells on different Pd core facets, where monolayer Pt atoms on Pd (100) and (110) facets can be seen as the defective structure of monolayer Pt atoms on Pd (111) facet. (b) Demonstration of the structural resemblance of the nearest neighbors in monolayer Pt shells on different Pd core facets, in which the structural model of monolayer Pt atoms on Pd single crystal (111) facet is employed in the respective EXAFS fitting of the standard monolayer Pt samples on different Pd single crystal facets to obtain almost the same results between the practically measured and the theoretically calculated parameters. Herein, the theoretical value of Pt−Pt and Pt−Pd bond distance is directly calculated from the atomic radius (R_{Pt}: 1.39 Å; R_{Pd}: 1.37 Å) without considering surface contraction, and the theoretical value of Pt−Pt and Pt−Pd coordination number is counted from structural units.

To validate the above structural resemblance, the structural model of monolayer Pt atoms on Pd single crystal (111) facet has been built according to the procedure in Figure S4, and then it is employed for EXAFS fitting of monolayer Pt atoms on Pd single crystal (111), (100), and (110) facets, respectively. Herein, various standard monolayer Pt samples on Pd single crystals[17] are prepared following the reported monolayer Cu mediator method,[18] and their XAS signal of Pt L_{III} edge is collected via a fluorescence mode at the beamline BL37XU in SPring-8 using a self-designed in situ electrochemical cell (Figure S5). Their fitting plots in both k and r space are shown in Figure S6. Figure 1b is the comparative results between the theoretical and the fitted parameters. As shown, on different Pd single crystals, theoretical Pt−Pt coordination numbers are 6, 4, and 2 on (111), (100), and (110) facets, respectively. Previous publication indicates the low coordination number of surface atoms will lead to the remarkably structural contraction.[19] Thus, on different facets, the practical Pt−Pt bond distance will decrease in the order of coordination number. In our fitted results (marked by the green dashed line), the structural contraction derived from the coordination number dependence has been quantitatively exhibited, where the longest Pt−Pt bond distance forms on Pd (111) facet and the shortest one generates on Pd (110) facet. Equally important, considering the small fluctuation of coordination number due to the surface defects in standard monolayer Pt samples (Figure S7), the obtained Pt−Pt coordination numbers are also in good agreement with the theoretical values.

From the above experiment, the employment of the standard monolayer Pt samples demonstrates that the self-built structural model of monolayer Pt atoms on Pd single crystal (111) facet is undoubtedly available. And, the self-built structural model can include all structural information of the nearest neighbors in monolayer Pt atoms on Pd single crystal (111), (100), and (110) facets. Thus, via the general structural model of monolayer Pt atoms on Pd single crystal (111) facet, EXAFS fitting of monolayer Pt shells on core nanoparticles with the short-range ordering structure is easily performed. It should be noted, the obtained structural parameters are average values of all structural information on different core facets.

Based on the above methodology, we further investigate monolayer Pt shells on a variety of Pd core nanoparticles (Figure S8 and S9, provided by Ishifuku Metal Industry, Japan) using in situ XAS. Herein, monolayer Pt shells on a variety of Pd nanoparticles are prepared following the reported monolayer Cu mediator method[18] (Figure S9), and their XAS signal of Pt L_{III} edge is collected via a fluorescence mode at the beamline BL01B1 and BL14B2 in SPring-8 using self-designed in situ electrochemical cell (Figure S5). Their EXAFS fitting plots in both k and r space based on the structural model of monolayer Pt atoms on Pd single crystal (111) facet are shown in Figure S10. Table 1 shows their different local structure of monolayer Pt shells induced by various Pd core nanoparticles. As observed, EXAFS fitting results reveal that Pt−Pt bond distance in monolayer Pt shells strongly depends on the particle size and surface roughness of Pd core

dx.doi.org/10.1021/ja312382h | J. Am. Chem. Soc. 2013, 135, 5938−5941

Table 1. Structural Parameters of the Nearest Neighbors in Monolayer Pt Shells on Different Pd Core Nanoparticles Fitted from the Corresponding EXAFS Using a General Structural Model of Monolayer Pt Atoms on Pd Single Crystal (111) Facet

pairs	N^a	R^b (Å)	DW^c (Å)	dE	$R_f{}^d$
On no. 1 Pd core, Size: 3.5 nm; Roughness^e: 0.53					
Pt−O	0.351 ± 0.519	1.939 ± 0.029	0.021 ± 0.193		
Pt−Pt	4.544 ± 1.815	2.708 ± 0.004	0.072 ± 0.039	9.117	0.611
Pt−Pd	4.233 ± 1.249	2.710 ± 0.003	0.069 ± 0.028		
On no. 2 Pd core, Size: 3.9 nm; Roughness: 0.43					
Pt−O	0.411 ± 0.674	1.973 ± 0.037	0.031 ± 0.138		
Pt−Pt	4.872 ± 1.677	2.715 ± 0.006	0.078 ± 0.039	9.949	0.551
Pt−Pd	4.018 ± 1.354	2.721 ± 0.004	0.074 ± 0.022		
On no. 3 Pd core, Size: 5.7 nm; Roughness: 0.39					
Pt−O	0.674 ± 0.788	1.980 ± 0.037	0.020 ± 0.151		
Pt−Pt	5.542 ± 1.930	2.724 ± 0.004	0.068 ± 0.045	8.597	0.535
Pt−Pd	3.951 ± 1.604	2.719 ± 0.003	0.064 ± 0.043		

$^a N$ is coordination number. $^b R$ is bond distance. ^{c}DW (Debye−Waller) is disorder factor. $^d R_f$ is fitting quality (residue). ^{e}Surface roughness is defined as the practical surface area/the theoretical one of Pd nanoparticles, and the calculation method is described in Supporting Information (SI).

nanoparticles, where the shortest Pt−Pt bond distance is formed on Pd core nanoparticles with the smallest particle size and the highest surface roughness. Further, for these Pd core nanoparticles, EXAFS fitting derived from the corresponding Pd K edge shows that three Pd samples have the almost same structure (Figure S11 and Table S2). It indicates that monolayer Pt structural control entirely depends on the particle size and surface structure of Pd core nanoparticles. In previous publications,[20,21] qualitative analysis and experimental results have found that a lateral compressive strain in a monolayer shell can be generated by the mismatch between shell and substrate atoms, the substrate surface curvature, and the contraction in substrate surface atoms in the radial direction. On Pd core nanoparticles, the mismatch extent between Pt shell and Pd core atoms is the same. However, a small particle size induces a large surface curvature,[22,23] and a high surface roughness implying the more surface atoms with the low coordination number generates a large radial contraction.[19] Thus, a small particle size and a high surface roughness facilitate the formation of a compressed monolayer Pt shell. Herein, the quantitative information of monolayer Pt local structure demonstrates the concept of tailoring monolayer Pt shell lattice strain via tuning core structure.

The quantitative lattice strain of monolayer Pt shells provides a tangible understanding on their different ORR activity (Figure S12) and the dependent correlation (Figure 2) between the lattice strain and the corresponding specific activity (at 0.90 V vs RHE) calculated from the Koutecky−Levich equation (Figure S13). As shown in Figure 2, the compression of Pt−Pt bond distance induces a remarkable increase in the specific activity toward ORR. Compared to the commercial Pt nanoparticles (0.20−0.25 mA cm^{-2}),[24] the greatest monolayer Pt shell induces a three-time increment in the specific activity. More importantly, these enhanced specific activities show a linear dependence on the lattice strain. In Pt alloyed or dealloyed systems,[9,10] other researchers have found volcano- or linear-type correlation between the lattice strain and the specific activity toward ORR. Compared to their findings, the linear dependence of monolayer Pt shell ORR activity on lattice strain is reasonable. Our quantitative correlation is also in good agreement with the theoretical explanation of the d-band model developed by Nøskov et al.[25] Thereinto, the strain effect induced d-band shift regulates the adsorption properties of rate-limiting intermediates in catalytic processes. For oxygen

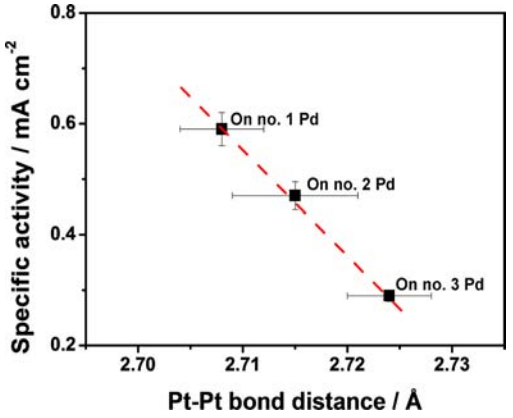

Figure 2. Lattice strain dependence of monolayer Pt shell ORR activity (at 0.9 V vs RHE). Herein, the error bar of Pt−Pt bond distance is calculated from EXAFS fitting, and the error bar of ORR activity is generated by over three measurements (size and roughness of Pd samples, no. 1: 3.5 nm, 0.53; no. 2: 3.9 nm, 0.43; no. 3: 5.7 nm, 0.39.).

reduction intermediates such as O and OH, it can be understood in a simple electron-interaction model in which the adsorbate valence p-level forms bonding and antibonding states with the metal d-band. Population of any antibonding state leads to Pauli repulsion, and thus the bond strength weakens. A downward shift of the d-band pulls more of the antibonding states below the Fermi level, which results in increasing occupation and weaker adsorbate bonding. Thus, in our experiments, the augment of the compression extent of Pt−Pt bond distance will generate a highly catalytic activity toward ORR. It should be noted, as for the eventual conclusion about the optimal lattice strain of monolayer Pt shells, an aborative tailoring of monolayer Pt structure is beyond the scope of this communication. It requires further study.

In summary, this work provides a feasible method for quantitatively assessing the lattice strain in monolayer Pt shells on core nanoparticles. Based on it, we demonstrate the feasibility of tailoring the lattice strain of monolayer Pt shell via tuning core structure and the linear dependence of monolayer Pt shell ORR activity on lattice strain. In the future, the finding in this work can be used to ascertain the complete correlation between the lattice strain of monolayer Pt shells and the resulting ORR activity, to predict the optimal lattice strain for

dx.doi.org/10.1021/ja312382h | J. Am. Chem. Soc. 2013, 135, 5938−5941

the maximum ORR activity and to guide the synthetic control of monolayer Pt shells.

■ ASSOCIATED CONTENT

Supporting Information

Sample preparation; XAS collection and EXAFS analysis; electrochemical testing. This material is available free of charge via the Internet at http://pubs.acs.org.

■ AUTHOR INFORMATION

Corresponding Author

wang.xiaoming.7u@kyoto-u.ac.jp

Notes

The authors declare no competing financial interest.

■ ACKNOWLEDGMENTS

This work was supported by Japan New Energy and Industrial Technology Development Organization (NEDO). In situ XAS was performed at SPring-8 (beamline BL01B1, BL14B2 and BL37XU) with the approval of Japan Synchrotron Radiation Research Institute (JASRI) (proposal no. 2012A1012, 2012A1020, 2011B1027, and 2011B1032).

■ REFERENCES

(1) Debe, M. K. *Nature* **2012**, *486*, 43.
(2) Gasteiger, H. A.; Markovic, N. M. *Science* **2009**, *324*, 48.
(3) Zhang, J.; Vukmirovic, M. B.; Xu, Y.; Mavrikakis, M.; Adzic, R. R. *Angew. Chem., Int. Ed.* **2005**, *44*, 2132.
(4) Wang, J. X.; Inada, H.; Wu, L. J.; Zhu, Y. M.; Choi, Y. M.; Liu, P.; Zhou, W. P.; Adzic, R. R. *J. Am. Chem. Soc.* **2009**, *131*, 17298.
(5) Zhou, W. P.; Yang, X.; Vukmirovic, M. B.; Koel, B. E.; Jiao, J.; Peng, G.; Mavrikakis, M.; Adzic, R. R. *J. Am. Chem. Soc.* **2009**, *131*, 12755.
(6) Shao, M.; Shoemaker, K.; Peles, A.; Kaneko, K.; Protsailo, L. *J. Am. Chem. Soc.* **2010**, *132*, 9253.
(7) Kitchin, J. R.; Nørskov, J. K.; Barteau, M. A.; Chen, J. G. *Phys. Rev. Lett.* **2004**, *93*, 156801.
(8) Mavrikakis, M.; Hammer, B.; Nørskov, J. K. *Phys. Rev. Lett.* **1998**, *81*, 2819.
(9) Strasser, P.; Koh, S.; Anniyev, T.; Greeley, J.; More, K.; Yu, C.; Liu, Z.; Kaya, S.; Nordlund, D.; Ogasawara, H.; Toney, M. F.; Nilsson, A. *Nat. Chem.* **2010**, *2*, 454.
(10) Mukerjee, S.; Srinivasan, S.; Soriaga, M. P.; McBreen, J. *J. Electrochem. Soc.* **1995**, *142*, 1409.
(11) Russell, A. E.; Rose, A. *Chem. Rev.* **2004**, *104*, 4613.
(12) Zhang, J.; Lima, F. H. B.; Shao, M. H.; Sasaki, K.; Wang, J. X.; Hanson, J.; Adzic, R. R. *J. Phys. Chem. B* **2005**, *109*, 22701.
(13) Vukmirovic, M. B.; Zhang, J.; Sasaki, K.; Nilekar, A. U.; Uribe, F.; Mavrikakis, M.; Adzic, R. R. *Electrochim. Acta* **2007**, *52*, 2257.
(14) Sasaki, K.; Wang, J. X.; Naohara, H.; Marinkovic, N.; More, K.; Inada, H.; Adzic, R. R. *Electrochim. Acta* **2010**, *55*, 2645.
(15) Price, S. W. T.; Speed, J. D.; Kannan, P.; Russell, A. E. *J. Am. Chem. Soc.* **2011**, *133*, 19448.
(16) Taufany, F.; Pan, C. J.; Rick, J.; Chou, H. L.; Tsai, M. C.; Hwang, B. J.; Liu, D. J.; Lee, J. F.; Tang, M. T.; Lee, Y. C.; Chen, C. I. *ACS Nano* **2011**, *5*, 9370.
(17) Hoshi, N.; Nakamura, M.; Kondo, S. *Electrochem. Commun.* **2009**, *11*, 2282.
(18) Brankovic, S. R.; Wang, J. X.; Adzic, R. R. *Surf. Sci.* **2001**, *474*, L173.
(19) Huang, W. J.; Sun, R.; Tao, J.; Menard, L. D.; Nuzzo, R. G.; Zuo, J. M. *Nat. Mater.* **2008**, *7*, 308.
(20) Adzic, R. R.; Zhang, J.; Sasaki, K.; Vukmirovic, M. B.; Shao, M.; Wang, J. X.; Nilekar, A. U.; Mavrikakis, M.; Valerio, J. A.; Uribe, F. *Top. Catal.* **2007**, *46*, 249.
(21) Xing, Y.; Cai, Y.; Vukmirovic, M. B.; Zhou, W. P.; Karan, H.; Wang, J. X.; Adzic, R. R. *J. Phys. Chem. Lett.* **2010**, *1*, 3238.
(22) Wang, L.; Roudgar, A.; Eikerling, M. *J. Phys. Chem. C* **2009**, *113*, 17989.
(23) Jiang, Q.; Liang, L. H.; Zhao, D. S. *J. Phys. Chem. B* **2002**, *105*, 6275.
(24) Gasteiger, H. A.; Kocha, S. S.; Sompalli, B.; Wagner, F. T. *Appl. Catal., B* **2005**, *56*, 9.
(25) Hammer, B.; Nørskov, J. K. *Adv. Catal.* **2000**, *45*, 71.